

## THE STABILITY AND CRYSTAL CHEMISTRY OF SYNTHETIC LOVERINGITE IN THE SYSTEM Ca–Mn–Ti–O UNDER STRONGLY REDUCING CONDITIONS

RONALD C. PETERSON<sup>1</sup>

*Department of Geological Sciences, Queen's University, Kingston, Ontario K7L 3N6*

IAN E. GREY, LACHLAN M.D. CRANSWICK AND CHRISTINA LI

*CSIRO Division of Minerals, Clayton 3169, Australia*

### ABSTRACT

The stability of loveringite,  $\text{Ca}(\text{Ca}, \text{Mn}, \text{Ti}^{3+}, \text{Ti}^{4+})_{21}\text{O}_{38}$ , in the system  $\text{CaO–MnO–Ti}_2\text{O}_3\text{–TiO}_2$  was studied as a function of oxygen fugacity at 1100°C. Loveringite was prepared as a pure or dominant phase at oxygen fugacities in the range  $10^{-15}$  to  $10^{-18}$  atm. At higher fugacities, the stable assemblage is rutile + pyrophanite + perovskite, whereas at lower fugacities, loveringite becomes unstable relative to mixtures of perovskite + pyrophanite +  $\text{Mn}_x\text{Ti}_{3-x}\text{O}_5$ . Results of electron-microprobe analyses and of wet-chemical analyses for  $\text{Ti}^{3+}$  show that the compositional variations in loveringite (in atoms per formula unit, *apfu*) are  $1.1 < \text{Ca} < 1.7$ ,  $1.8 < \text{Mn} < 3.2$ ,  $2.4 < \text{Ti}^{3+} < 5.6$  and  $13.2 < \text{Ti}^{4+} < 14.4$ . The dominant mode of compositional variation involves the charge-coupled mechanism of substitution  $\text{Mn}^{2+} + \text{Ti}^{4+} \rightleftharpoons 2\text{Ti}^{3+}$ . Crystal-chemical variations in synthetic loveringite were studied using Rietveld refinement of powder X-ray data. The unit-cell parameters are strongly correlated with the Ca and Mn contents. Calcium in excess of 1 *apfu* is ordered at the largest octahedral site, *M1*. Samples with higher Mn contents have Mn ordered at the *M1* site and the tetrahedral site *T*. Strongly reduced samples, with low manganese contents, have Mn preferentially at the *T* site, and  $\text{Ti}^{3+}$  at *M1*.

*Keywords:* loveringite, crichtonite, powder diffraction, Rietveld refinement, ilmenite.

### SOMMAIRE

Nous avons étudié la stabilité de la loveringite,  $\text{Ca}(\text{Ca}, \text{Mn}, \text{Ti}^{3+}, \text{Ti}^{4+})_{21}\text{O}_{38}$ , dans le système  $\text{CaO–MnO–Ti}_2\text{O}_3\text{–TiO}_2$  en fonction de la fugacité de l'oxygène à 1100°C. On prépare la loveringite comme composé pur ou dominant à une fugacité de l'oxygène dans l'intervalle  $10^{-15}$  à  $10^{-18}$  atm. Aux fugacités supérieures, l'assemblage stable est rutile + pyrophanite + pérovskite, tandis qu'aux fugacités plus faibles, la loveringite est déstabilisée au profit de mélanges de pérovskite + pyrophanite +  $\text{Mn}_x\text{Ti}_{3-x}\text{O}_5$ . Les résultats d'analyses à la microsonde électronique et d'analyses chimiques par voie humide pour établir la teneur en  $\text{Ti}^{3+}$  montrent que les variations en composition de la loveringite (exprimées en atomes par unité formulaire) sont  $1.1 < \text{Ca} < 1.7$ ,  $1.8 < \text{Mn} < 3.2$ ,  $2.4 < \text{Ti}^{3+} < 5.6$  et  $13.2 < \text{Ti}^{4+} < 14.4$ . Le mode dominant de variation en composition implique le mécanisme couplé  $\text{Mn}^{2+} + \text{Ti}^{4+} \rightleftharpoons 2\text{Ti}^{3+}$ . Nous nous sommes servis d'affinements de données de diffraction X par méthode de Rietveld pour étudier les variations cristallochimiques dans la loveringite synthétique. Les paramètres réticulaires montrent une forte corrélation avec la teneur en Ca et Mn. Le Ca dépassant un atome par unité formulaire se trouve dans le site octaédrique le plus spacieux, *M1*. Les échantillons contenant des teneurs plus élevées en Mn ont cet élément dans le site *M1* et dans le site tétraédrique *T*. Dans les échantillons fortement réduits, ayant de faibles teneurs en manganèse, le Mn se trouve de préférence dans le site *T*, et le  $\text{Ti}^{3+}$ , dans le site *M1*.

*Mots-clés:* loveringite, crichtonite, diffraction X sur poudre, affinement par méthode de Rietveld, ilménite.

<sup>1</sup>E-mail address: peterson@geol.queensu.ca

## INTRODUCTION

Loveringite,  $(Ca,REE)(Ti,Fe,Cr)_2O_{38}$ , is a relatively common accessory titanate mineral in layered igneous intrusions (Campbell & Kelly 1978). It is a member of the crichtonite group of minerals,  $AB_{19}T_2O_{38}$ , having calcium as the dominant *A* cation. In such structures, the *A* cations occupy 12-coordinated sites in a closest-packed framework of oxygen atoms, with small cations occupying four independent octahedral sites, *M*, and a tetrahedral site, *T* (Grey *et al.* 1976b). The variety of cation sites provides structural flexibility for the accommodation of a wide range of elements, including uranium, thorium, zirconium and the rare-earth elements (*REE*). This flexibility has led to the consideration of loveringite-type phases as host phases for the immobilization of radionuclides in nuclear waste (Buykx *et al.* 1988). The compositional adaptability of loveringite is further extended by the possibility of calcium (and *REE*) occupying both the 12-coordinated *A* site and the largest of the octahedral sites, *M1*. Full occupancy of both the *A* and *M1* sites by calcium has been demonstrated in a structure refinement of the synthetic phase  $Ca_2Zn_4Ti_{16}O_{38}$  (Gatehouse & Grey 1983). Loveringite has been shown to be stable at high pressures (30 kbar at 1000°C) by Green & Pearson (1987), who have suggested that the loveringite – davidite (*A* = *REE*) solid-solution series may be an important accessory repository for the rare-earth elements in the upper mantle.

The present study of synthetic loveringite developed from laboratory work on a new process to upgrade ilmenite ( $FeTiO_3$ ). In Australia, ilmenite is commercially upgraded to synthetic rutile (SR) by the Becher process (Becher *et al.* 1965). The process involves reduction of the ilmenite with coal at ~1100–1150°C to give metallic iron plus titanium oxides, followed by accelerated rusting and removal of the iron. The new process, called SREP (Synthetic Rutile Enhancement Process; Ellis *et al.* 1994), is a modification of the Becher process, and is intended to improve the processing of ilmenite concentrates containing impurities other than iron. In SREP, a borate flux is added to the ilmenite during reduction. Fluxes tested include ulexite, colemanite, kernite, hydroboracite, kurnakovite, inderite and szaibelyite. The flux incorporates the impurity elements and allows them to be removed easily by leaching, after the iron-removal step. When fluxes containing calcium were tested, it was found that a loveringite-type phase was present in the reduction product. This phase was not attacked in the leaching step, and so it represented a limitation in terms of the quality of the synthetic rutile (SR) obtained.

Modifications to the SREP process to avoid or minimize the formation of loveringite requires a knowledge of the stability field of the loveringite-type phase. In designing an experimental program to determine the phase-stability domain of loveringite, use was made of published information on the chemical reactions involved in the Becher SR process (Grey & Reid 1974).

Natural ilmenite feedstocks to the SR process contain manganese as the major impurity. In the strongly reducing conditions used, most of the iron oxide is converted to the metal, and MnO then becomes a phase-controlling component in the reduced oxide assemblage. At the same time, a significant proportion of the titanium is reduced to the trivalent state. To a good approximation, the phase assemblages present in the reduced oxide product can then be described within the phase system  $MnO-TiO_2-Ti_2O_3$ . We have previously reported phase relations in this system as a function of the fugacity of oxygen (Grey *et al.* 1976a). By including CaO as a component, these studies can be extended to include a loveringite-type phase. The temperature (1100°C) and reducing conditions used were chosen to be relevant to SREP operating conditions, and a small amount of  $B_2O_3$  was added to simulate the borate flux. We report here the preparation and phase chemistry of synthetic loveringite phases formed in the system  $CaO-MnO-TiO_2-Ti_2O_3$  at oxygen fugacities in the range  $10^{-14}$  to  $10^{-18.5}$  atm.

## EXPERIMENTAL

*Syntheses*

The experimental procedures used for the phase studies are similar to those used for our recently reported study on synthetic lindsleyite,  $BaMn_3Ti_{18}O_{38}$  (Peterson & Grey 1995). Starting materials for the phase studies were analytical reagent  $CaCO_3$ ,  $Mn_2O_3$  and  $TiO_2$  (anatase form). The  $Mn_2O_3$  was prepared by thermal decomposition of reagent grade  $MnCl_2 \cdot 4H_2O$  in air at 600°C. Weighed mixtures of the starting materials were pressed into 2 g pellets and contained in molybdenum foil boats for heating experiments at 1100°C in controlled gaseous reducing atmospheres. Oxygen fugacities in the range  $10^{-14}$  to  $10^{-18.5}$  atm were established using mixtures of  $CO_2$  and  $H_2$  or  $H_2O$  and  $H_2$ . The latter mixture was used at the lowest fugacities to avoid carbon deposition. The samples were generally given at least two heat treatments at a particular oxygen fugacity, with intermediate grinding. Many of the compositions were re-equilibrated at different oxygen fugacities.

For the majority of the synthesis experiments, a small amount of boron was added, as either calcium borate or  $B_2O_3$ . The purpose of this addition was two-fold: to more closely reproduce the conditions pertaining to the SREP process, where a borate flux is added, and to aid the crystal growth of the equilibrium phases so they could be unambiguously analyzed by electron-microprobe techniques. The starting compositions and equilibration conditions used are reported in Table 1. Conditions are given only for those runs where loveringite is a dominant phase in the equilibrated product. Associated minor phases, as identified by powder X-ray diffraction (PXRD), are also reported in Table 1.

TABLE 1. STARTING COMPOSITIONS OF LOVERINGITE, AND ACCESSORY PHASES IN EQUILIBRATED PRODUCTS

Sample	log $f(\text{O}_2)$	Starting Mixture (wt%)				Accessory Phases
		CaCO <sub>3</sub>	Mn <sub>2</sub> O <sub>3</sub>	TiO <sub>2</sub>	B <sub>2</sub> O <sub>3</sub>	
73	-18.0	6.8	10.7	80.3	2.2	M <sub>2</sub> O <sub>3</sub> (minor), Pph (trace)
69b	-18.0	6.8	13.7	77.3	2.2	M <sub>2</sub> O <sub>3</sub> (minor), Pph (minor)
36b	-18.0	7.0	7.8	85.2	0	Ti <sub>2</sub> O <sub>3</sub> (trace)
49d	-18.0	8.8	9.7	79.3	2.2	Prv (trace)
50d	-18.0	8.8	10.7	78.3	2.2	Pph (trace), Prv (trace)
51d	-18.0	8.8	11.7	77.2	2.2	Pph (minor), Prv (minor)
52d	-18.0	8.8	12.7	76.3	2.2	Pph (minor), Prv (minor)
53d	-18.0	8.8	13.7	75.3	2.2	Pph (minor), Prv (minor)
73d	-17.3	6.8	10.7	80.3	2.2	(pure loveringite)
70d	-17.3	6.8	12.7	78.3	2.2	MnTiO <sub>3</sub> (minor)
69d	-17.3	6.8	13.7	77.3	2.2	M <sub>2</sub> O <sub>3</sub> (trace), Pph (minor)
8b	-17.1	6.8	9.7	83.5	0	(pure loveringite)
33a	-17.1	6.8	12.0	81.2	0	M <sub>2</sub> O <sub>3</sub> (trace), Pph (trace)
14b	-17.1	7.0	8.9	84.1	0	Ti <sub>4</sub> O <sub>7</sub> (trace)
29b	-17.1	7.3	12.0	80.7	0	Pph (trace), Prv (trace)
30a	-17.1	8.4	11.0	80.6	0	Pph (trace), Prv (minor)
49b	-16.7	8.8	9.7	79.3	2.2	rutile (trace), Prv (trace)
50	-16.7	8.8	10.7	78.3	2.2	rutile (trace)
51	-16.7	8.8	11.7	77.2	2.2	rutile (trace)
54c	-16.7	8.8	14.7	74.3	2.2	Pph (minor), Prv (minor)
71	-16.5	6.8	11.7	79.3	0	rutile (>minor)
18a	-16.5	9.5	11.0	79.5	0	Prv (minor), Pph (trace)
60	-15.3	8.8	9.7	79.3	2.2	rutile (>minor)
61	-15.3	8.8	10.7	78.3	2.2	rutile (minor)
62	-15.3	8.8	11.7	77.3	2.2	rutile (>minor)
63	-15.3	8.8	12.7	76.3	2.2	rutile (>minor), Pph (trace)
64	-15.3	8.8	13.7	75.3	2.2	rutile (minor), Pph (trace)
65	-15.3	8.8	14.7	74.3	2.2	rutile (minor), Pph (minor)
9b	-15.2	8.6	13.6	77.8	0	(pure loveringite)
4g	-15.2	9.0	13.7	77.1	0	(pure loveringite)
15c	-15.0	6.5	12.5	79.9	1.1	rutile (>minor), Pph (minor)
15b	-15.0	9.7	10.3	78.9	1.1	rutile (>minor), Prv (minor)
15a	-15.0	9.7	15.4	73.8	1.1	rutile (minor), Pph (minor)

Pph=pyrophanite, Prv=perovskite, trace=<2%, minor=2-10%

### Powder X-ray-diffraction studies

PXRD was used for the routine identification of phases in the equilibrated products and to provide intensity data for structure refinements by the Rietveld method (Rietveld 1969). Samples for PXRD were prepared by grinding the reaction pellets in a tungsten carbide mill and back-pressing the powders into an aluminum sample holder. Measurements of diffracted intensities were made using a Philips 1050 goniometer with a PW1710 controller and using a long fine-focus copper tube operated at 40 kV and 40 mA. The diffractometer was configured with a 1° divergent slit, 0.2 mm receiving slit, 1° scatter slit, incident- and diffracted-beam Soler slits, and a diffracted-beam curved graphite monochromator.

For the Rietveld refinements, intensity data were collected at 22°C, from 10° to 150° 2θ, with a step size of 0.025° and a variable counting time (VCT) strategy (Madsen & Hill 1994). The total counting time was 28.8 or 43.2 ks per run. Powder-diffraction step-scan intensities may be obtained from the Depository of Unpublished Data, CISTI, National Research Council of Canada, Ottawa, Ontario K1A 0S2.

### Rietveld refinements

Least-squares refinements were carried out using the Rietveld programs SR2 and SR5. These are local modifications of the code by Hill & Howard (1986) and Wiles & Young (1981), which take account of VCT data sets and quantitative phase-analysis of multiphase mixtures. Profile-refinement parameters included a scale factor, two pseudo-Voigt shape parameters, a 2θ zero parameter, a three-term full-width at half-maximum function (Caglioti *et al.* 1958), calculated for nine half-widths on either side of the peak maxima, a peak-asymmetry parameter for peaks less than 50° 2θ, and unit-cell parameters. The background was modeled using a five-parameter polynomial fit. Scattering curves for neutral atoms were taken from International Tables for X-ray Crystallography (1974).

Refinements were initiated using the reported atomic coordinates for loveringite (Gatehouse *et al.* 1978). Assignment of cation site-occupancies made use of the relatively large differences in size between the different cations Ca<sup>2+</sup> > Mn<sup>2+</sup> > Ti<sup>3+</sup> > Ti<sup>4+</sup> and the known relative volumes of the cation sites from published work (Gatehouse *et al.* 1979). Calcium was assigned to the A site. If the microprobe results showed more than one Ca per formula unit, the excess calcium was assigned to the largest M site, M(1), consistent with previous single-crystal-refinement results for Ca<sub>2</sub>Zn<sub>4</sub>Ti<sub>16</sub>O<sub>38</sub> (Gatehouse & Grey 1983). Manganese was assigned progressively to the M(1) site, then T, then M(2), depending on the amount available. Titanium was ordered at the sites M(2) to M(4). Full occupancy of all metal sites was maintained in the refinements for

### Analyses

Wavelength-dispersion X-ray analyses of phases in polished cross-sections were carried out using a Cameca Camebax electron microprobe operated at 15 kV and 20 nA. Rutile, TiO<sub>2</sub> (TiKα), manganese metal (MnKα) and wollastonite, CaSiO<sub>3</sub> (CaKα) were used as standards.

The single-phase loveringite produced was analyzed for trivalent titanium by dissolving the ground sample in a H<sub>2</sub>SO<sub>4</sub> – HF solution containing excess ferric iron, then titrating the ferrous iron formed (Ti<sup>3+</sup> + Fe<sup>3+</sup> ⇌ Ti<sup>4+</sup> + Fe<sup>2+</sup>) against potassium dichromate. The method was calibrated using reduced titanium oxides of known composition. From tests, it was confirmed that manganese does not interfere with the analyses for Ti<sup>3+</sup>.

Selected samples were analyzed by X-ray fluorescence to check if the Ca:Mn:Ti contents in the products remained the same as were used in the starting mixtures.

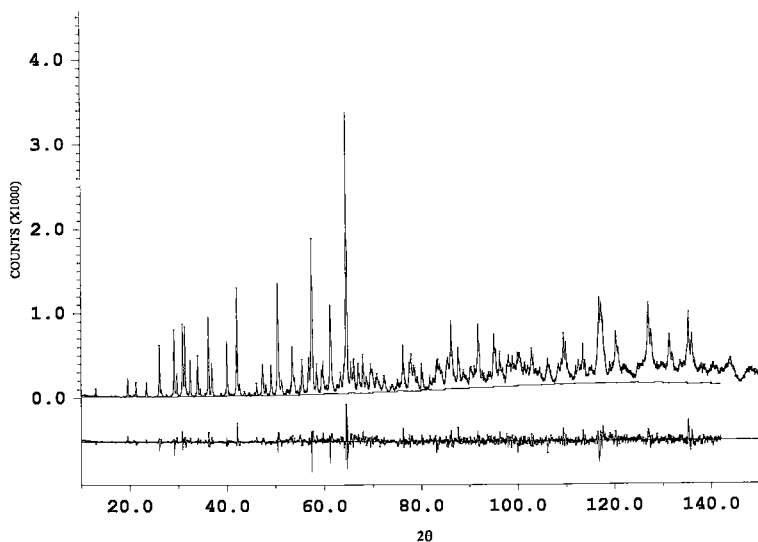


FIG. 1. An example of the diffraction data used (sample 36B). The variable-counting-time data and calculated line are indistinguishable in this plot. The lower line represents the observed counts minus the calculated counts.

most samples. However, for samples prepared under strongly reducing conditions, and containing the lowest contents of calcium and manganese, site-occupancy refinements suggested variations to the above scheme of order, including incomplete occupancy of the *T* site. In these samples, the site occupancies were established using both site-occupancy refinements and valence-sum calculations. The isotropic displacement parameters for the oxygen atoms were constrained to be equal in the refinements while individual values of *B* for the metal atoms were refined. The small amounts (typically ~1–3 wt%) of accessory phases rutile, perovskite ( $\text{CaTiO}_3$ ) and pyrophanite ( $\text{MnTiO}_3$ ) were included in the refinements. The final  $R_{wp}$  and  $R_b$  values obtained were in the ranges 9.6 to 16.2% and 2.8 to 5.2%, respectively. Plots of the difference between calculated and observed intensities (Fig. 1) showed no significant discrepancies.

## RESULTS AND DISCUSSION

### Phase equilibria

Experimental conditions that led to a loveringite-type phase as the dominant phase are listed in Table 1. Small amounts of accessory phases that were in equilibrium with loveringite at the conditions used (identified by PXRD) are also reported in Table 1. Strongly reducing conditions, with oxygen fugacities lower than  $10^{-14}$  atm, were required to stabilize loveringite. At less reducing conditions, loveringite was unstable relative to

the phase assemblage rutile + perovskite + pyrophanite. Similar behavior, *i.e.*, stability only at low oxygen fugacities, was found for synthetic lindsleyite in the system Ba–Mn–Ti–O (Peterson & Grey 1995). Loveringite was formed as a single or dominant phase at oxygen fugacities in the range  $10^{-15}$  atm to  $10^{-16}$  atm. At  $f(\text{O}_2) = 10^{-18.5}$  atm, the phase assemblage comprised mainly perovskite + pyrophanite +  $M_3\text{O}_5$ , where  $M_3\text{O}_5$  is a solid solution of the type  $\text{Mn}_x\text{Ti}_{3-x}\text{O}_5$ . The solid solution is formed by substitution of the type  $2\text{Ti}^{3+} \rightleftharpoons \text{Mn}^{2+} + \text{Ti}^{4+}$ . We have previously reported on the stability field for this solid solution as a function of oxygen fugacity at 1200°C (Grey *et al.* 1976a). It is worth noting that whereas loveringite containing  $\text{Mn}^{2+}$  needs strongly reducing conditions (presence of  $\text{Ti}^{3+}$ ) for stability; we were also able to prepare loveringite-type phases in the system Ca–Mn–Ti–O under oxidizing conditions where both  $\text{Mn}^{2+}$  and  $\text{Mn}^{3+}$  were present.

For calcium-rich and manganese-rich compositions, perovskite and pyrophanite, respectively, were found as coexisting phases with loveringite over the full range of oxygen fugacities used. Rutile or reduced rutile phases were also found to occur over the full range of fugacities for the titanium-rich compositions.  $M_3\text{O}_5$  was found as an accessory phase only at oxygen fugacities lower than  $10^{-17}$  atm, and at the lower manganese and calcium contents in the reaction mixtures. This is consistent with our previous studies of the system  $\text{MnO-TiO}_2\text{-Ti}_2\text{O}_3$ , which showed that  $M_3\text{O}_5$  is unstable relative to an assemblage of reduced rutile + pyrophanite for  $x > 0.65$  (Grey *et al.* 1976a).

An interesting observation from Table 1 is that for borate-free compositions, excess  $TiO_2$  led to the formation of accessory reduced rutile-type phases such as  $Ti_6O_{11}$  and  $Ti_4O_7$ , whereas for all the runs incorporating a borate flux component, the only titanium oxide observed by PXRD is rutile. This observation can be explained by incorporation of boron into the rutile structure by a charge-compensation mechanism given by  $3Ti^{4+} \approx 3Ti^{3+} + B^{3+}$  (interstitial). Up to 1.1 wt%  $B_2O_3$  and 7.5 wt%  $Ti_2O_3$  can be incorporated into rutile at 1100°C and at  $f(O_2) = 10^{-17}$  atm (Grey *et al.* 1997). The coupled substitution of boron and trivalent titanium stabilizes the rutile structure-type to oxygen fugacities that are two orders of magnitude lower than occurs in the pure system  $Ti-O$ . Electron-microprobe studies showed that the amount of boron incorporated into loveringite and the other accessory phases ( $M_3O_5$ , pyrophanite, perovskite) was at or below the limit of detection (0.1 wt%  $B_2O_3$ ).

### Electron-microprobe data and phase chemistry

Table 2 gives the results of electron-microprobe analyses, presented as oxides, for loveringite phases formed in the samples listed in Table 1. The atomic formulae are also given in Table 2, calculated on the basis of 38 oxygen atoms and with all metal atom sites fully occupied, which is consistent with the structural formula  $AM_{19}T_2O_{38}$ . With the manganese present only as  $Mn^{2+}$  (Grey *et al.* 1976b), charge balance is achieved by adjusting the  $Ti^{3+}:Ti^{4+}$  ratio. The resulting calculated  $TiO_2$  and  $Ti_2O_3$  contents are shown in Table 2. The calculated distribution of tri- and tetravalent titanium results in analytical totals that are predominantly in the range 99.5 to 100.5%. The range of  $Ti_2O_3$  calculated for loveringite is 10 to 24%. This can be compared with  $Ti_2O_3$  ranges of 0 to 47% in the binary system  $Ti-O$ , and 22 to 33% in  $Mn_xTi_{3-x}O_5$  for equivalent ranges of oxygen fugacity (Grey *et al.* 1974, 1976a).

The assignment of  $Ti^{3+}$  and  $Ti^{4+}$  from the electron-microprobe data was checked by direct chemical analysis of single-phase samples for trivalent titanium. Good agreement was obtained between the measured and calculated compositions, for example 10.6%  $Ti_2O_3$  (measured) versus 11.2%  $Ti_2O_3$  (calc.) in one sample, and 22.4%  $Ti_2O_3$  (measured) versus 23.3%  $Ti_2O_3$  (calc.) for another. For the sample that had the lowest combined Ca + Mn, the measured value of 20.4%  $Ti_2O_3$  was significantly lower than the calculated value of 24.3%  $Ti_2O_3$ . This may indicate the presence of cation vacancies in this sample.

The proportion of trivalent titanium, in atoms per formula unit (*apfu*), is shown as a function of  $f(O_2)$  in Figure 2. The values range from 2.4 *apfu* at the least reducing conditions to 5.6 *apfu* at the lowest oxygen fugacity used. At any particular  $f(O_2)$  value, there is a relatively wide spread of  $Ti^{3+}$ , which relates to the different amounts of manganese and calcium available,

TABLE 2. RESULTS OF ELECTRON-MICROPROBE ANALYSES (wt%) AND CALCULATED FORMULAE OF LOVERINGITE

sample	log $f(O_2)$	$TiO_2$	$Ti_2O_3$	MnO	CaO	total	Ca	Mn	$Ti^{3+}$	$Ti^{4+}$
49d	-18.0	66.5	19.1	9.9	5.0	100.	1.49	2.31	4.40	13.80
49d-Priv	-18.0	67.0	18.5	9.2	5.8	100.	1.72	2.15	4.25	13.88
49d	-18.0	68.4	20.3	9.5	5.0	101.	1.47	2.21	4.44	13.68
49d	-18.0	68.1	19.4	9.6	5.1	100.	1.52	2.24	4.48	13.76
49d	-18.0	65.9	19.7	9.3	5.2	100.	1.54	2.18	4.55	13.73
50d-Pph	-18.0	65.7	18.9	9.7	4.8	100.	1.42	2.27	4.62	13.69
50d	-18.0	65.3	20.1	9.6	4.7	99.6	1.41	2.26	4.67	13.67
50d-Priv	-18.0	66.6	18.8	9.8	5.2	100.	1.53	2.30	4.34	13.83
73	-18.0	64.0	22.3	8.8	4.4	99.5	1.33	2.07	5.20	13.40
73	-18.0	64.5	21.8	9.2	4.4	99.9	1.30	2.17	5.07	13.47
69b-Pph	-18.0	65.8	19.9	9.9	4.7	100.	1.39	2.31	4.60	13.70
69b	-18.0	65.7	19.7	10.3	4.4	100.	1.30	2.41	4.58	13.71
69b	-18.0	65.5	19.8	10.6	4.1	100.	1.21	2.48	4.81	13.69
36b	-18.0	63.7	23.3	7.8	5.1	99.8	1.50	1.80	5.40	13.30
36b	-18.0	63.6	23.2	7.8	5.0	99.6	1.50	1.80	5.40	13.30
36b	-18.0	63.5	24.2	8.1	4.4	100.	1.30	1.50	5.60	13.20
36b	-18.0	62.3	21.8	7.9	5.0	97.0	1.50	1.80	5.20	13.40
73d-Pph	-17.3	67.0	18.7	10.8	4.6	101.	1.35	2.51	4.29	13.86
73d	-17.3	64.7	21.9	9.2	4.4	100.	1.30	2.17	5.06	13.47
73d-Pph	-17.3	65.5	19.5	10.3	4.2	99.9	1.26	2.43	4.61	13.70
73d	-17.3	63.7	22.2	9.1	4.2	99.2	1.25	2.16	5.19	13.41
73d	-17.3	64.1	22.1	9.2	4.2	98.6	1.26	2.17	5.13	13.43
70d	-17.3	65.5	19.9	10.5	4.1	100.	1.22	2.47	4.62	13.69
70d	-17.3	65.5	19.8	10.0	4.6	99.6	1.36	2.36	4.55	13.72
70d	-17.3	66.8	18.7	11.6	3.9	100.	1.15	2.70	4.30	13.85
14b	-17.1	64.0	20.3	9.5	3.8	99.6	1.15	2.25	5.20	13.40
14b	-17.1	63.2	21.2	9.2	4.3	98.3	1.30	2.20	5.00	13.50
29b	-17.1	66.2	18.0	11.9	3.8	99.9	1.10	2.80	4.20	13.90
29b	-17.1	67.4	17.3	12.1	3.7	100.	1.10	2.90	4.00	14.00
30a	-17.1	66.7	18.1	11.7	3.7	100.	1.20	2.70	4.20	13.90
30a-Pph	-17.1	66.1	17.0	10.9	4.5	99.5	1.40	2.60	4.00	14.00
33a	-17.1	65.7	18.9	11.0	4.0	99.6	1.20	2.60	4.40	13.90
49b	-16.7	66.5	18.5	9.6	5.4	100.	1.61	2.25	4.29	13.85
49b	-16.7	65.6	19.6	9.6	4.9	99.7	1.45	2.27	4.56	13.72
50	-16.7	66.8	18.2	10.5	4.9	100.	1.44	2.46	4.20	13.90
50-r	-16.7	66.3	19.5	8.9	4.6	99.3	1.37	2.35	4.55	13.72
50r	-16.7	67.2	18.0	10.4	5.1	100.	1.51	2.42	4.14	13.93
50-Priv	-16.7	64.7	20.2	10.0	4.2	99.0	1.27	2.36	4.72	13.84
50	-16.7	67.1	17.4	10.4	5.2	100.	1.54	2.44	4.04	13.98
71	-16.5	67.7	16.6	12.1	4.2	100.	1.24	2.84	3.84	14.08
71-flux	-16.5	67.1	16.7	11.9	4.2	99.9	1.26	2.80	3.89	14.06
71-flux	-16.5	67.4	17.1	11.9	4.1	100.	1.22	2.80	3.89	14.02
71	-16.5	67.6	16.4	11.9	4.2	100.	1.24	2.92	3.67	14.16
18a	-16.5	67.6	16.4	11.9	4.3	100.	1.30	2.80	3.80	14.10
60	-15.3	70.3	11.5	13.2	5.3	100.	1.59	3.10	2.67	14.68
60	-15.3	70.7	11.1	13.3	5.4	100.	1.61	3.11	2.58	14.72
60	-15.3	69.7	11.9	12.9	5.4	99.7	1.64	2.98	2.77	14.62
63-r	-15.3	70.0	11.5	13.3	5.1	99.9	1.53	3.14	2.67	14.66
63-Pph	-15.3	69.7	11.8	13.1	5.2	99.8	1.54	3.09	2.75	14.63
63-r	-15.3	70.4	11.2	13.2	5.4	100.	1.59	3.11	2.60	14.70
62	-15.3	69.0	13.6	12.3	5.1	100.	1.52	2.90	3.15	14.42
62	-15.3	70.1	10.5	13.1	5.5	99.2	1.65	3.12	2.48	14.77
62	-15.3	69.3	12.7	12.7	5.1	99.8	1.53	3.00	2.95	14.52
61-r	-15.3	70.1	11.7	12.9	5.4	100.	1.61	3.03	2.72	14.64
61	-15.3	69.5	12.2	12.9	5.1	99.7	1.54	3.04	2.84	14.58
61	-15.3	69.8	11.6	12.8	5.4	99.7	1.62	3.03	2.71	14.65
15a	-15.0	71.1	10.3	13.4	5.6	100.	1.68	3.16	2.38	14.81
15b	-15.0	70.2	11.4	13.0	5.4	100.	1.61	3.08	2.86	14.67
15c	-15.0	70.1	11.2	13.4	5.2	99.7	1.54	3.16	2.60	14.70

Suffixes: Pph:  $MnTiO_3$ , Priv:  $CaTiO_3$ , r:  $TiO_2$ , flux: indicates composition of loveringite close to that of these materials.

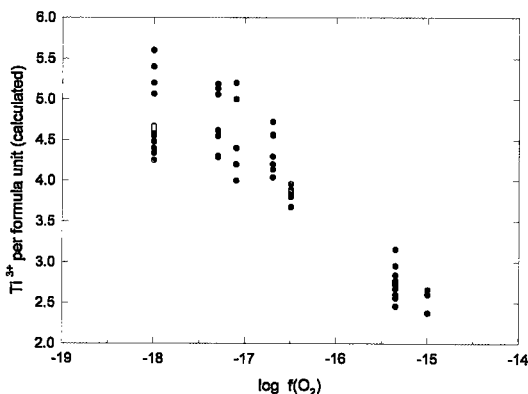


FIG. 2. Concentration of  $Ti^{3+}$  (in *apfu*) versus  $\log f(O_2)$  for synthetic loveringite. The proportion of  $Ti^{3+}$  is calculated from the electron-microprobe data on the basis of the formula  $AM_{19}T_2O_{38}$ .

depending on the bulk composition and accessory phases present. The spread of  $Ti^{3+}$  contents decreases considerably at the higher oxygen fugacities.

Loveringite was analyzed from different grains in each sample, and from points adjacent to phase boundaries with accessory phases (Table 2), to illustrate the compositional variation within individual samples. The points adjacent to phase boundaries are indicated by an abbreviated suffix that denotes the accessory phase. There are small compositional variations within individual samples, but the variations do not appear to be systematically related to the character of the associated phases. A more likely explanation for the minor compositional heterogeneity is a variation in element partitioning between loveringite and the borate-rich liquid owing to volatilization of boron from liquid regions near the surface of the sample pellets. This was confirmed by scanning electron microscopy on sectioned pellets. The quenched borate liquid was observed to be distributed in interstices between titanate grains, and was depleted near the pellet surfaces. No evidence of crystalline borates was found in PXRD patterns, and so it is assumed that the liquid borate was converted to a glass phase during quenching of the reaction products. The composition of the borate glass varies considerably in the various samples: observed ranges are 15–29% CaO, 18–35% MnO, 10–12%  $TiO_2$  and 33–41%  $B_2O_3$ , with the MnO and CaO inversely correlated.

The electron-microprobe data for loveringite all lie within the  $CaTiO_3$ – $MnTiO_3$ – $Ti_2O_3$ – $TiO_2$  subsystem of the quaternary system Ca–Mn–Ti–O. Figure 3 shows tie lines linking the various compositions of loveringite and the associated accessory phases. The constraints imposed by adherence to the crystallographic formula  $AM_{19}T_2O_{38}$  require that the loveringite compositions all lie in a plane parallel to the  $CaTiO_3$ – $MnTiO_3$ – $Ti_2O_3$  base of the quaternary subsystem. Within this plane, the analyzed compositions are bounded by the four compositions  $Ca_2Mn_3Ti_{17}O_{38}$ ,  $Ca_2MnTi_{19}O_{38}$ ,  $CaMn_4Ti_{17}O_{38}$  and  $CaMn_2Ti_{19}O_{38}$  (Fig. 4). The observed ranges (in *apfu*) are 1.1 to 1.7 for Ca, 1.8 to 3.2 for Mn and 17.2 to 18.8 for Ti. In Figure 4, arrows indicate the directions in which the analytical points would be arranged if the substitutions followed each of the three possible cation-substitution schemes,  $Ca^{2+} \rightleftharpoons Mn^{2+}$ ,  $Ca^{2+} + Ti^{4+} \rightleftharpoons 2Ti^{3+}$  and  $Mn^{2+} + Ti^{4+} \rightleftharpoons 2Ti^{3+}$ . It is clear that the spread of analytical points is not consistent with a single scheme of substitution.

Further information on the nature of the cation substitutions is obtained from plots of Mn and Ca *versus*  $Ti^{3+}$  and Mn *versus* Ca (as *apfu*) (Figs. 5, 6). The calculation of the  $Ti^{3+}$  contents requires a 1:2 correlation of Mn + Ca to  $Ti^{3+}$ , but it imposes no restrictions on the Ca–Mn correlations. The manganese content is much more strongly correlated with  $Ti^{3+}$  (Fig. 5, slope =  $-2.1$ ,  $r^2 = 0.88$ ) than is Ca (slope =  $-0.1$ ,  $r^2 = 0.30$ ), such that

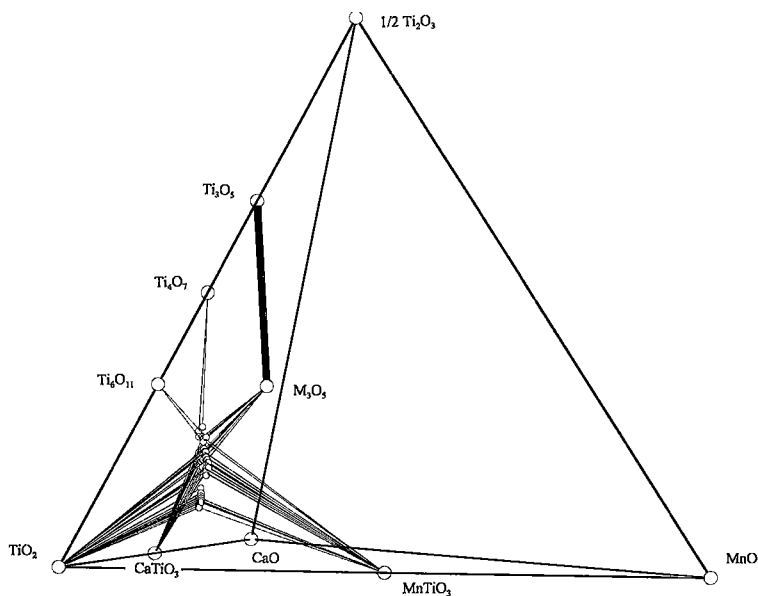


FIG. 3. A representation of the quaternary system CaO–MnO– $TiO_2$ – $1/2Ti_2O_3$ . The compositions of loveringite compositions, obtained from electron-microprobe analyses, are represented as spheres with tie-lines to the other phases observed for each run.

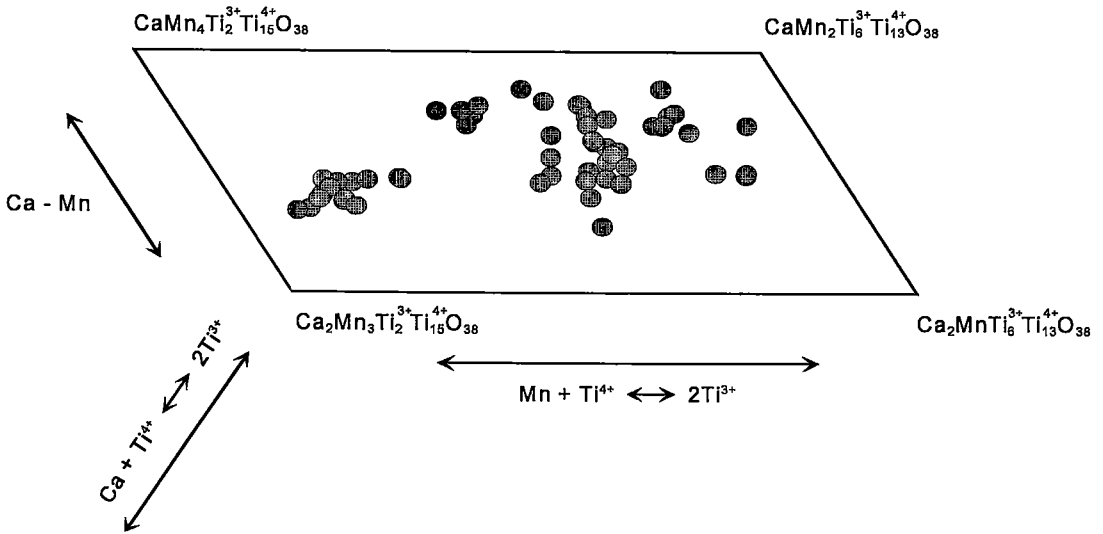


FIG. 4. A section through the quaternary system, bounded by the compositions  $\text{Ca}_2\text{Mn}_3\text{Ti}_{17}\text{O}_{38}$ ,  $\text{Ca}_2\text{MnTi}_{19}\text{O}_{38}$ ,  $\text{CaMn}_4\text{Ti}_{17}\text{O}_{38}$  and  $\text{CaMn}_2\text{Ti}_{19}\text{O}_{38}$ . The compositions of synthetic loveringite obtained from the electron-microprobe analyses are shown. Arrows indicate possible substitution vectors.

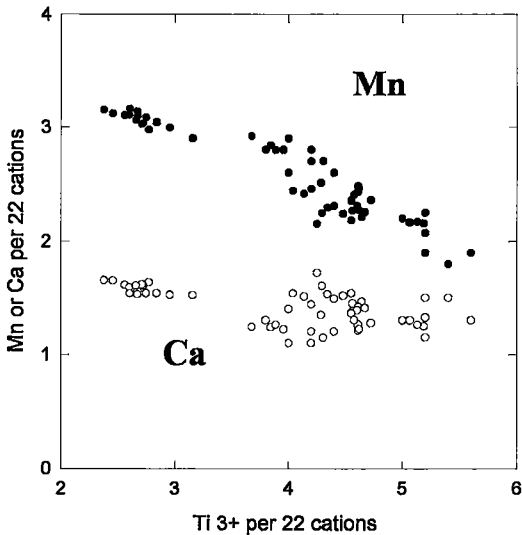


FIG. 5. Plots of concentration of Mn versus that of  $\text{Ti}^{3+}$  (filled circles) and of Ca versus that of  $\text{Ti}^{3+}$  (open circles). Results, in *apfu*, are from electron-microprobe analyses.

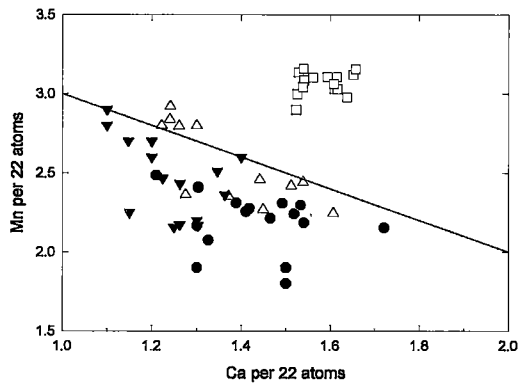


FIG. 6. Plots of concentration of Mn versus that of Ca (in *apfu*) from electron-microprobe analyses. Open square:  $f(\text{O}_2) = 10^{-15.3}$  or  $10^{-15.0}$ , open triangle:  $f(\text{O}_2) = 10^{-16.5}$ , solid triangle:  $f(\text{O}_2) = 10^{-17.3}$ , and solid circle:  $f(\text{O}_2) = 10^{-18}$  atm.

the dominant pattern of substitution is  $\text{Mn}^{2+} + \text{Ti}^{4+}$  for  $2\text{Ti}^{3+}$ . The Mn versus Ca results (Fig. 6) are differentiated with respect to the experimental  $f(\text{O}_2)$  by using different symbols. Weak to moderate correlations are

present in the results at intermediate  $f(\text{O}_2)$  values of  $10^{-16.5}$  and  $10^{-17.3}$  atm (slope =  $-1.3$  and  $-1.4$ ,  $r^2 = 0.23$  and  $0.60$ , respectively), but there are no clear correlations at the two  $f(\text{O}_2)$  extremes.

Comparison of the compositions of the synthetic loveringite prepared in this study with compositions reported in the literature shows that the major difference is the much higher titanium content of the synthetic samples. Natural occurrences of loveringite are generally found in igneous layered complexes. Published electron-microprobe results (Lorand *et al.* 1987, Campbell & Kelly 1978, Cameron 1978) on samples from a number of localities show that the titanium contents are in the range 56 to 73 wt% TiO<sub>2</sub>. In contrast, the combined tri- and tetravalent titanium oxides in our synthetic samples, expressed as TiO<sub>2</sub>, are in the range 82 to 90%. However, considering only the TiO<sub>2</sub> component, the range is 62 to 71% TiO<sub>2</sub>, which is consistent with the published results for natural samples. This indicates that Ti<sub>2</sub>O<sub>3</sub> is playing the same role as does Cr<sub>2</sub>O<sub>3</sub> + Fe<sub>2</sub>O<sub>3</sub> in the mineral samples.

#### Rietveld refinements: crystal chemistry

Loveringite has rhombohedral symmetry ( $R\bar{3}$ ), and its structure is based on closest-packed layers of anions having a nine-layer stacking sequence (*hhchhchc...*). Calcium atoms are ordered in sites where a closest-packed anion is missing from the *c*-stacked layers to give a layer composition CaO<sub>12</sub>. The small metal atoms are ordered in one tetrahedral interstice and four different octahedral interstices to give the (ideal) formula CaM<sub>19</sub>T<sub>2</sub>O<sub>38</sub>. The layered nature of the arrangement of polyhedra is apparent in Fig-

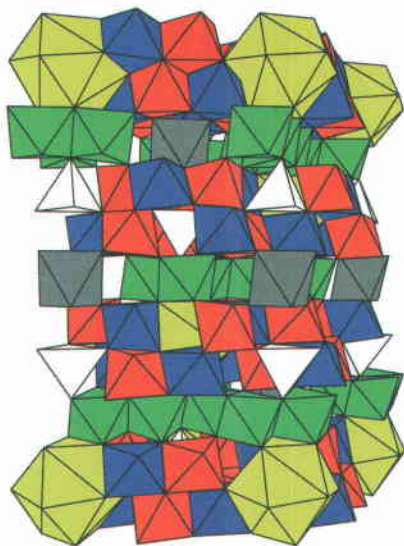


FIG. 7. A polyhedron representation of the structure of loveringite showing the layered arrangement of the coordination polyhedra in this closest-packed oxide, with M1 and M2 forming one layer, and the A-site, T, M3 and M4 polyhedra forming a double layer. The shading of the polyhedra in the figure is as follows: A yellow, T white, M1 grey, M2 green, M3 blue, and M4 red.

ure 7, where a layer of octahedra composed of M(1) and M(2) alternates with a double layer containing the T, M(3) and M(4) sites.

The crystal-chemical variations in synthetic loveringite were studied by carrying out Rietveld refinements on selected samples that consist of a single phase or contain only small amounts of accessory phases. The samples were selected to cover the full range of compositional variations. Given the limitations of PXRD data for such complex structures, and the similar electron scattering by Ca, Mn and Ti, refinement of metal-atom site populations was of limited value. Use was made of the known relative sizes of the different sites from published results on refined loveringite-related structures to assign site occupancies, as described in the Experimental section. The number of Ca, Mn and Ti atoms to be distributed was obtained from the electron-microprobe results, or from the XRF analyses for single-phase samples.

Refined parameters for the samples 36b and 9b, having near-maximum and minimum Ti<sup>3+</sup> concentrations, are compared in Table 3. The metal-atom site occupancies in the two samples are shown in Table 4, together with the results of valence-sum calculations, obtained with the empirical bond-length – bond-strength parameters of Brown & Wu (1976). For the sample 9b, the assignment of the largest cations progressively into the A, then M1, then T, then M2 sites gave good agreement between the calculated valence-sums and the formal valences of the atoms occupying the M and T sites. However, for the strongly reduced sample 36b, having the lowest Mn content, a closer agreement between calculated and formal valence-states was obtained with the manganese ordered in the T site only and with Ca + Ti<sup>3+</sup> occupying the M1 site. The valence-sum calculations gave poor agreement with the formal valence for calcium in the A site for both samples. The divalent calcium is too small to occupy the center of the 12-coordinated site, and presumably takes up various positions slightly displaced from the center to satisfy its coordination requirements. This is reflected for the isotropic temperature-factor for the A site, as shown in Table 3, and previously observed in Ca<sub>2</sub>Zn<sub>4</sub>Ti<sub>16</sub>O<sub>38</sub> (Gatehouse & Grey 1983).

Refinement indices, unit-cell data and site occupancies are given in Table 5 for a range of loveringite compositions. Full data concerning the refinements of all samples are available from the Depository of Unpublished Data, CISTI, National Research Council, Ottawa, Ontario K1A 0S2. The site occupancies that gave the best overall fit to the data are given in Table 5. They must be considered with caution owing to the limitations of the PXRD data for refinement of such complex structures.

In Table 5 are listed average bond-lengths for the polyhedra containing the A, T and M sites. Given that the error associated with the mean bond-lengths is typically 0.01 Å, the only significant trend with composition appears to be associated with the T site.

TABLE 3. PARAMETERS OF REFINED STRUCTURE OF SYNTHETIC LOVERINGITE, SAMPLES 9b [ $f(\text{O}_2) = 10^{-15.2}$  atm] AND 36b [ $f(\text{O}_2) = 10^{-18.0}$  atm]

Sample 9b: $\text{Ca}_{1.6}\text{Mn}_{3.1}\text{Ti}^{3+}_{2.6}\text{Ti}^{4+}_{14.7}\text{O}_{38}$					Sample 36b: $\text{Ca}_{1.6}\text{Mn}_{1.8}\text{Ti}^{3+}_{5.4}\text{Ti}^{4+}_{13.3}\text{O}_{38}$				
$a = 10.4200(1) \text{ \AA}$ , $c = 20.9413(2) \text{ \AA}$					$a = 10.4027(2) \text{ \AA}$ , $c = 20.8817(5) \text{ \AA}$				
$R_{\text{wp}} = 12.4\%$ , $R_g = 4.5\%$					$R_{\text{wp}} = 13.9\%$ , $R_g = 5.2\%$				
Site	x	y	z	B ( $\text{\AA}^2$ )	x	y	z	B ( $\text{\AA}^2$ )	
A	0	0	0	2.3(2)	0	0	0	2.7(3)	
T	0	0	0.3098(2)	0.51(6)	0	0	0.3116(3)	1.0(1)	
M1	0	0	1/2	0.6(1)	0	0	1/2	0.7(2)	
M2	0.1884(3)	0.1463(3)	0.1645(2)	0.58(4)	0.1854(4)	0.1434(4)	0.1653(2)	0.51(5)	
M3	0.8129(3)	0.2428(3)	0.3908(1)	0.51(5)	0.9133(5)	0.2429(5)	0.3904(2)	0.55(9)	
M4	0.0753(3)	0.7604(4)	0.3988(1)	0.57(5)	0.0749(5)	0.7581(5)	0.3989(2)	0.40(6)	
O1	0.865(1)	0.082(1)	0.4345(5)	0.81(6)	0.871(2)	0.054(2)	0.4329(6)	0.59(7)	
O2	0.703(1)	0.500(1)	0.4408(6)	"	0.709(2)	0.503(1)	0.4445(6)	"	
O3	0.350(1)	0.259(1)	0.5586(5)	"	0.354(2)	0.259(2)	0.5585(6)	"	
O4	0.597(1)	0.558(1)	0.5499(4)	"	0.597(2)	0.580(2)	0.5500(6)	"	
O5	0.052(1)	0.205(1)	0.3372(6)	"	0.055(1)	0.204(1)	0.3407(7)	"	
O6	0.370(1)	0.287(1)	0.3399(5)	"	0.370(1)	0.289(1)	0.3387(8)	"	
O7	0	0	0.2123(8)	"	0	0	0.2121(1)	"	

TABLE 4. BOND-VALENCE SUMS FOR SYNTHETIC LOVERINGITE, SAMPLES 9b [ $f(\text{O}_2) = 10^{-15.2}$  atm] AND 36b [ $f(\text{O}_2) = 10^{-18.0}$  atm]

Sample 9b: $\text{Ca}_{1.6}\text{Mn}_{3.1}\text{Ti}^{3+}_{2.6}\text{Ti}^{4+}_{14.7}\text{O}_{38}$				36b: $\text{Ca}_{1.6}\text{Mn}_{1.8}\text{Ti}^{3+}_{5.4}\text{Ti}^{4+}_{13.3}\text{O}_{38}$			
Site occupancies	S <sup>a</sup>	s <sub>i</sub> <sup>b</sup>		Site occupancies	S <sup>a</sup>	s <sub>i</sub> <sup>b</sup>	
A = Ca	2.0	1.6		A = Ca	2.0	1.5	
T = Mn	2.0	2.1		T = 0.9Mn+0.1Ti <sup>3+</sup>	2.1	2.1	
M1 = 0.6Ca+0.4Mn	2.0	2.0		M1 = 0.5Ca+0.5Ti <sup>3+</sup>	2.5	2.4	
M2 = 0.1Mn+0.5Ti <sup>3+</sup> +0.4Ti <sup>4+</sup>	3.3	3.3		M2 = 0.7Ti <sup>3+</sup> +0.3Ti <sup>4+</sup>	3.3	3.4	
M3 = Ti <sup>4+</sup>	4.0	3.8		M3 = Ti <sup>4+</sup>	4.0	3.8	
M4 = Ti <sup>4+</sup>	4.0	3.8		M4 = Ti <sup>4+</sup>	4.0	3.8	

<sup>a</sup> formal valence at metal atom site. <sup>b</sup> s: valence sum calculated with the parameters of Brown & Wu (1976).

TABLE 5. RESULTS OF RIETVELD REFINEMENT OF SYNTHETIC LOVERINGITE, AND MEAN BOND-DISTANCES ( $\text{\AA}$ ) FOR THE POLYHEDRA

Sample	9b	50	49b	36b	30a	8b	29b	18a	33a
log $f(\text{O}_2)$	-15.2	-16.7	-16.7	-18.0	-17.1	-17.1	-17.1	-16.5	-17.1
Ca (apfu)	1.6	1.5	1.55	1.5	1.3	1.2	1.2	1.3	1.2
Mn (apfu)	3.1	2.4	2.25	1.8	2.7	2.0	2.8	2.8	2.6
Ti (apfu)	17.3	18.1	18.2	18.7	18.0	18.8	18.0	17.9	18.2
Rwp	12.4	12.2	11.3	13.9	16.2	14.8	15.4	9.6	16.2
R <sub>g</sub>	4.5	3.9	3.2	5.2	5.2	4.5	5.2	2.8	4.8
a ( $\text{\AA}$ )	10.4200(1)	10.4105(1)	10.4081(1)	10.4027(2)	10.4100(2)	10.4034(2)	10.4099(2)	10.4052(2)	10.4074(2)
c ( $\text{\AA}$ )	20.9413(2)	20.9163(4)	20.9148(4)	20.8817(6)	20.8890(5)	20.8582(6)	20.8694(6)	20.8548(6)	20.8439(6)
V ( $\text{\AA}^3$ ) <sup>a</sup>	658.35	654.4	654.0	652.3	653.5	651.7	653.3	651.7	651.7
c/a	2.010	2.009	2.009	2.007	2.0085	2.005	2.005	2.004	2.003
SOF**	1.0Mn	0.95Mn+0.05Ti	0.9Mn+0.1Ti	0.9Mn+0.1Ti	1.0Mn	0.75Mn+0.25Ti	1.0Mn	1.0Mn	0.9Mn+0.1Ti
T	0.6Ca+0.4Mn	0.5Ca+0.5Mn	0.55Ca+0.45Mn	0.5Ca+0.5Ti	0.3Ca+0.7Mn	0.2Ca+0.3Ti+0.5Mn	0.2Ca+0.8Mn	0.3Ca+0.7Mn	0.2Ca+0.8Mn
M1	0.11Mn+0.89Ti	1.0Ti	1.0Ti	1.0Ti	1.0Ti	1.0Ti	1.0Ti	1.0Ti	1.0Ti
M2	Ti								
<A-O>***	2.78	2.77	2.76	2.82	2.81	2.79	2.78	2.77	2.80
<T-O>	2.02	2.02	2.04	2.02	2.04	2.01	2.02	2.01	2.02
<M1-O>	2.27	2.26	2.23	2.20	2.23	2.21	2.23	2.22	2.23
<M2-O>	2.02	2.02	2.01	2.00	2.01	2.00	2.01	2.00	2.00
<M3-O>	1.97	1.99	1.98	1.98	1.98	1.97	1.98	1.97	1.98
<M4-O>	1.98	1.95	1.96	1.98	1.97	1.98	1.97	1.98	1.97

<sup>a</sup>V = volume of rhombohedral cell. <sup>\*\*</sup>SOF for A = 1.0Ca and for M3, M4 = 1.0Ti for all samples. <sup>\*\*\*</sup>mean esd ~ 0.01Å

The  $\langle M1-O \rangle$  mean distance shows a moderate correlation with the amounts of Ca and Mn. The  $a$  and  $c$  parameters are also correlated with the amounts of these

two largest cations. The correlations for  $a$ ,  $c$  and  $\langle M1-O \rangle$  are shown in Figures 8 and 9, respectively.

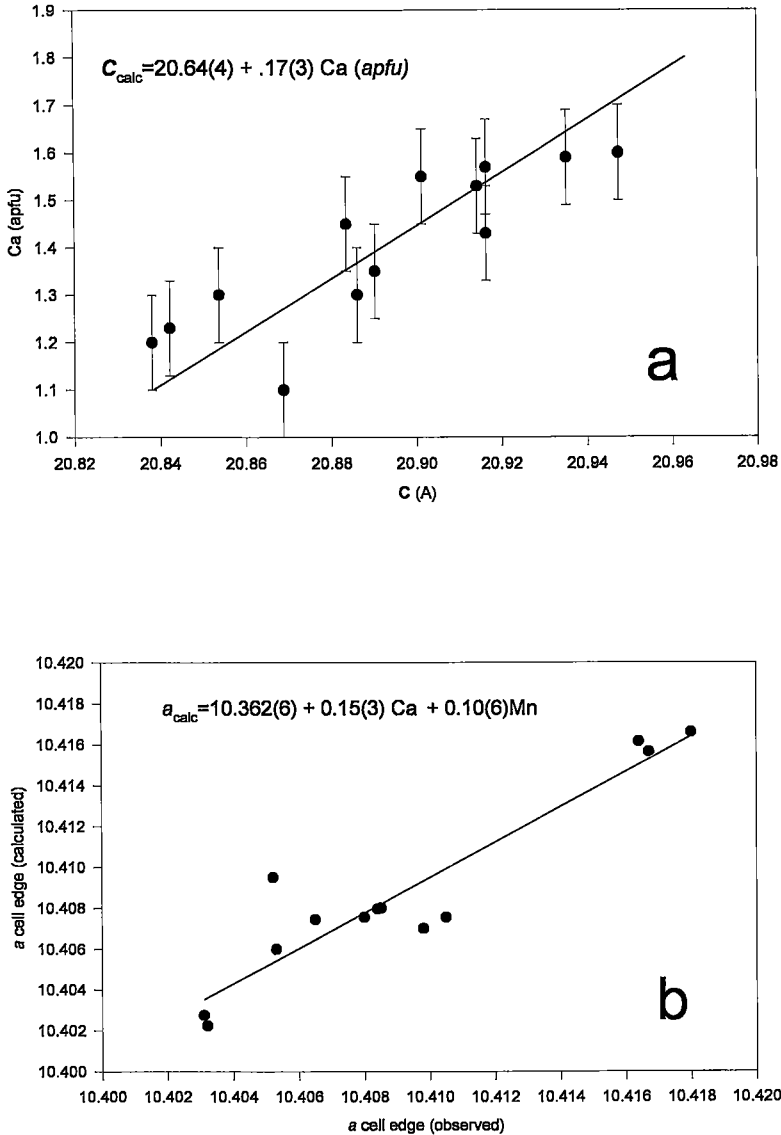


FIG. 8. The unit-cell parameters of the hexagonal cell are related to the amount of calcium and manganese found in the structure. (a) The  $c$  cell edge (in Å) is most closely related to the amount of calcium in the structure ( $r^2 = 0.74$ ), whereas (b) the  $a$  cell edge (also in Å) is related to the calcium and manganese content ( $r^2 = 0.87$ ).

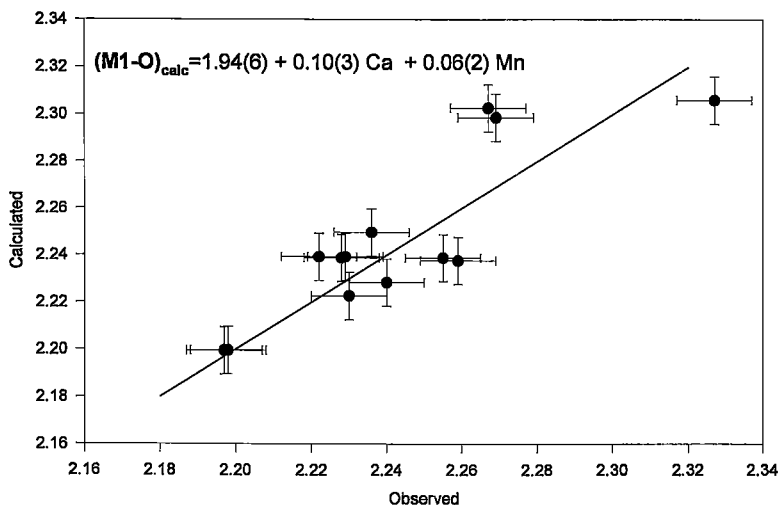


FIG. 9. The  $M1-O$  bond length (in Å) is related to the amount of calcium and manganese per formula unit by the equation given.

## CONCLUSIONS

Synthetic loveringite phases,  $Ca(Ca,Mn,Ti)_{21}O_{38}$ , can be prepared in the system  $CaO-MnO-Ti_2O_3-TiO_2$  only at oxygen fugacities lower than about  $10^{-14}$  atm. Single-phase (or close to single-phase) samples were prepared in the oxygen fugacity range  $10^{-14}$  to  $10^{-18}$  atm and for compositions in the range 1.1–1.7 *apfu* Ca, 1.8–3.2 *apfu* Mn, 2.4–5.6 *apfu*  $Ti^{3+}$  and 13.2–14.4 *apfu*  $Ti^{4+}$ . The principal mode of compositional variation results from the substitution  $Mn^{2+} + Ti^{4+} \rightleftharpoons 2Ti^{3+}$ . For all compositions, calcium is ordered at both the *A* and *M1* sites. For compositions with low contents of trivalent titanium, manganese is ordered at the *M1* and *T* sites. For the more strongly reduced, low-manganese samples, manganese preferentially orders in the *T* site, and trivalent titanium, in the *M1* site. The principal compositional difference between the synthetic phases and natural occurrences of loveringite is the much higher titanium contents of the synthetic material. In the strongly reduced synthetic samples,  $Ti_2O_3$  plays the role of the  $Fe_2O_3$  and  $Cr_2O_3$  found in mineral samples.

## ACKNOWLEDGEMENTS

We thank RGC Mineral Sands for their support of this project. We are grateful to Raul Lobo and Peter Leavens for their comments. We also thank R.F. Martin for editorial assistance. The work was supported, in part, by an NSERC grant to RCP.

## REFERENCES

- BECHER, R.G., CANNING, R.G., GOODHEART, B.A. & UUSNA, S. (1965): A new process for upgrading ilmenitic mineral sands. *Proc. Aust. Inst. Mining Metall.* **214**, 21–44.
- BROWN, I.D. & WU, KANG KUN (1976): Empirical parameters for calculating cation–oxygen bond valences. *Acta Crystallogr.* **B32**, 1957–1959.
- BUYKX, W., HAWKINS, K., LEVINS, D.M., MITAMURA, H.S., SMART, R.ST.C., STEVENS, G.T., WATSON, K.G., WEEDON, D. & WHITE, T.J. (1988): Titanite ceramics for the immobilization of sodium-bearing high-level nuclear waste. *J. Am. Ceram. Soc.* **71**, 678–688.
- CAGLIOTTI, G., PAOLETTI, A. & RICCI, F.P. (1958): Choice of collimators for a crystal spectrometer for neutron diffraction. *Nucl. Instrum. Methods* **3**, 223–228.
- CAMERON, E.N. (1978): An unusual titanium-rich oxide mineral from the eastern Bushveld Complex. *Am. Mineral.* **63**, 37–39.
- CAMPBELL, I.H. & KELLY, P.R. (1978): The geochemistry of loveringite, a uranium–rare-earth bearing accessory phase from the Jemberlana Intrusion of Western Australia. *Mineral. Mag.* **42**, 187–193.
- ELLIS, B.A., HARRIS, H.R. & HUDSON, R.L. (1994): The reduction of radionuclides in titaniferous feedstocks. *Proc. 11th Industrial Minerals Int. Congress (Berlin, Germany)*.

- GATEHOUSE, B.M. & GREY, I.E. (1983): The crystal structure of  $\text{Ca}_2\text{Zn}_4\text{Ti}_{16}\text{O}_{38}$ . *J. Solid State Chem.* **46**, 151-155.
- \_\_\_\_\_, \_\_\_\_\_, CAMPBELL, I.H. & KELLY, P.R. (1978): The crystal structure of loveringite – a new member of the crichtonite group. *Am. Mineral.* **63**, 28-36.
- \_\_\_\_\_, \_\_\_\_\_ & KELLY, P.R. (1979): The crystal structure of davididite. *Am. Mineral.* **64**, 1010-1017.
- GREEN, T.H. & PEARSON, N.J. (1987): High pressure, synthetic loveringite – davidite and its rare earth element geochemistry. *Mineral. Mag.* **51**, 145-149.
- GREY, I.E., LI, C., MACCRAE, C.M. & BURSILL, L.A. (1997): Boron incorporation into rutile: phase equilibria and structure considerations. *J. Solid State Chem.* **127**, 240-247.
- \_\_\_\_\_, \_\_\_\_\_ & REID, A.F. (1974): A thermodynamic study of iron in reduced rutile. *J. Solid State Chem.* **11**, 120-127.
- \_\_\_\_\_, \_\_\_\_\_ & \_\_\_\_\_ (1976a): Phase equilibria in the system  $\text{MnO-TiO}_2\text{-Ti}_2\text{O}_3$  at 1473°K. *J. Solid State Chem.* **17**, 343-352.
- \_\_\_\_\_, LLOYD, D.J. & WHITE, J.S., JR. (1976b): The structure of crichtonite and its relationship to senaite. *Am. Mineral.* **61**, 1203-1212.
- \_\_\_\_\_, \_\_\_\_\_ & REID, A.F. (1974): Reaction sequence in the reduction of ilmenite. 3. Reduction in a rotary kiln; an X-ray diffraction study. *Inst. Mining Metall. Trans., Sect. C*, **83**, 39-46.
- HILL, R.J. & HOWARD, C.J. (1986): A computer program for Rietveld analysis of fixed-wavelength X-ray and neutron powder diffraction patterns. *Aust. Atomic Energy Comm., Rep. M112*.
- INTERNATIONAL TABLES FOR X-RAY CRYSTALLOGRAPHY, vol. IV (1974): The Kynoch Press, Birmingham, U.K.
- LORAND, J.-P., COTTIN, J.-Y. & PARODI, G.C. (1987): Occurrence and petrological significance of loveringite in the western Laouni layered complex, southern Hoggar, Algeria. *Can. Mineral.* **25**, 683-693.
- MADSEN, I.C. & HILL, R.J. (1994): Collection and analysis of powder diffraction data with near constant counting statistics. *J. Appl. Crystallogr.* **27**, 385-392.
- PETERSON, R.C. & GREY, I.E. (1995): Preparation and structure refinement of synthetic  $\text{Ti}^{3+}$ -containing lindsleyite,  $\text{BaMn}_3\text{Ti}_{18}\text{O}_{38}$ . *Can. Mineral.* **33**, 1083-1089.
- RIETVELD, H.M. (1969): A profile refinement method for nuclear and magnetic structures. *J. Appl. Crystallogr.* **2**, 65-71.
- WILES, D.B. & YOUNG, R.A. (1981): A new computer program for Rietveld analysis of X-ray powder diffraction patterns. *J. Appl. Crystallogr.* **14**, 149-151.

Received July 14, 1997, revised manuscript accepted May 2, 1998.